processes

MDPI

Article

Development of a Novel Dimensionless Relationship to Describe Mass Transfer in Ladles Due to Bottom Gas Injection

Zhiyong Liu and Alberto N. Conejo *

School of Metallurgical and Ecological Engineering, University of Science and Technology Beijing, Beijing 100083, China; liuzhiyong@xs.ustb.edu.cn

* Correspondence: aconejonava@hotmail.com; Tel.: +86-178-1213-2203

Abstract: In the quest to design reactors with a higher productivity, their mixing efficiency should be highly improved. The mass transfer coefficient is a parameter that measures the rate of the refining rates and has been extensively investigated in the past; however, most of the correlations developed in steelmaking are based on the effect of the gas flow rate or its alternative form, stirring energy. The gas flow rate can play a big role in mass transfer but there are many more variables involved. This work has investigated the combined effect of five variables on the mass transfer coefficient due to bottom gas injection with two injection devices: the gas flow rate, the radial position and the separation angle of the porous plugs, the slag thickness, and the ladle aspect ratio. A novel expression in a dimensionless form has been developed, which accurately predicts the mass transfer coefficient. The expression proposed indicates that increasing the gas flow rate, the slag thickness, the ladle aspect ratio, and the separation angle also increases the mass transfer coefficient. On the contrary, increasing the radial position away from the center affects mass transfer, especially at high gas flow rates. Based on the experimental data and their practical application, an optimum layout for the injection of gas is suggested to optimize both mass transfer and the mixing intensity of liquid steel.

Keywords: mass transfer coefficient; bottom gas injection; gas flow rate; radial position; ladle aspect ratio; slag thickness; mixing

check for updates

Academic Editor: Evangelos Tsotsas

Received: 28 November 2024
Revised: 19 December 2024
Accepted: 20 December 2024
Published: 24 December 2024

Citation: Liu, Z.; Conejo, A.N. Development of a Novel Dimensionless Relationship to Describe Mass Transfer in Ladles Due to Bottom Gas Injection. *Processes* **2025**, *13*, 5. https://doi.org/10.3390/pr13010005

Copyright: © 2024 by the authors. Licensee MDPI, Basel, Switzerland. This article is an open access article distributed under the terms and conditions of the Creative Commons Attribution (CC BY) license (https://creativecommons.org/licenses/by/4.0/).

1. Introduction

The role of mixing phenomena on the rate of steel refining has become even more critical under the conditions of a higher concentration of impurities in the raw materials. Barrington [1] reported an increase in the average P content from 480 to 670 ppm from 1998 to 2019 in a representative group of iron ores. Many countries have large reserves of low-quality iron ores, for example, China has almost four billion tons of oolitic hematite ore, a low-quality iron ore with an Fe content of 35–40%, and significant phosphorous of 0.4–1.8% P [2]. In the case of sulfur, its main source is from coal. The increasing trend in impurities in raw materials is in opposition to the decreasing trend on the limits to produce high-quality steels. Holappa [3] has summarized this trend indicating the requirements of super-clean steels as P < 30 ppm and S < 10 ppm.

Mixing phenomena in ladles have been extensively investigated [4] in the past 50 years; however, the main mixing phenomenon investigated has been the optimization of chemical mixing in liquid steel using measurements of mixing time. Due to the small thickness of the slag layer, its mixing conditions have never been measured or calculated before and still remain a challenge in this field. Despite this limitation, the effect of bottom gas injection on

the removal of impurities from liquid steel to the slag has also been investigated. Conejo [5] provided an extensive literature review in ladles on the effect of bottom gas injection on the mass transfer coefficient. This work put forward that a large number of variables have an influence on the mass transfer coefficient, the gas flow rate in particular has the strongest effect; however, the nozzle radial position, its separation angle slag thickness, and the ladle aspect ratio have been poorly investigated, becoming the motivation for the present work. Since the previous review provides an extensive review, the following is a brief summary and update on the subject.

In 1987, Kim and Fruehan [6] were the first to report that a central gas injection with one nozzle produced higher refining rates, but at the same time, the poor mixing conditions in the molten bath indicated that the mixing conditions with the same layout are different for molten metal and molten slag, in other words, good mixing conditions for liquid steel are unfavorable for mass transfer. The same authors [7] also derived an expression to describe a critical gas flow rate, Q_{cr}, to reach slag emulsification, indicating that increasing the depth of molten steel and the slag/metal density difference also increase the value of Q_{cr}. Slag emulsification is the reason for a drastic change in mass transfer due to an increment in the slag/metal interface.

In an extensive analysis of mass transfer, Abel et al. [8] in 1995 developed two expressions to describe the volumetric mass transfer coefficient as a function of four dimensionless groups, for water models and for industrial reactors. The following expression corresponds to water models:

$$\frac{kA}{V_s^{\frac{1}{3}}D} = 10^{0.61}\left(\frac{U_p^2\rho_m H_m}{\sigma_{ms}}\right)^{1.32}\left(\frac{\varepsilon}{\rho_m U_p^3 d_b^2}\right)^{1.07}\left(\frac{\Delta\rho}{\rho_m}\right)^{-1.06}\left(\frac{V_s^{\frac{1}{3}}}{H_m}\right)^{0.88} \quad (1)$$

The term on the LHS is the Sherwood number and the two first terms on the RHS are the Weber and Power numbers, respectively. This equation can be recast as follows:

$$kA = 76.2\frac{\varepsilon^{1.07}\rho_m^{1.06}V_s^{0.63}H_m^{0.3}D}{Q_{g,T,P}^{0.19}\Delta\rho^{0.8}\sigma_{ms}^{1.32}d_b^{1.95}(1-\alpha)^{0.05}} \quad (2)$$

where V_s is the oil volume, U_p is the plume velocity, H_m is the height of water, $\Delta\rho$ is the density difference in the fluids, ρ_m is the density of liquid steel, σ_{ms} is the surface tension at the interface, ε is the stirring energy, D is a diffusion coefficient, d_b is the bath diameter, and α is the gas holdup.

Joubert et al. [9] carried out mass transfer experiments in a cubic vessel, with the gas flow rate as the main variable and the other experimental conditions similar to Kim and Fruehan [6]. They reported a linear relationship between the Sherwood and Froude numbers:

$$\frac{kL}{4D} = 5000\frac{U_p^2}{\sqrt{gH_m}} \quad (3)$$

where L is the width of the cube. The plume velocity was estimated with the expression $U_p = \left(g^2Q\right)^{\frac{1}{5}}$. These authors did not mention this, but the equation appears to be valid below a critical Froude number, most probably below slag emulsification.

Wang et al. [10] carried out mass transfer experiments in a water model representing top gas injection in the BOF. They described mass transfer with three dimensionless groups: Re, Sc, and Sh. The Sherwood number was defined in terms of the average diameter of the oil droplets (kd_o/D), the Schmidt number in terms of the dynamic viscosity of water ($\mu_m/\rho_m D$), and the Reynolds number ($U_m\rho_m d_o/\mu_m$), as follows:

$$Sh = 5.78 \times 10^{-3} Re^{0.43} Sc^{0.33} \quad (4)$$

An important observation in this work, for practical purposes, is that increasing the velocity of the fluids (liquid metal and liquid slag) has an even more enhancing effect on mass transfer in comparison with changes in their chemical composition.

Our research group has also reported several papers on this subject [11–13]: Hoang [14] reported that the mixing time in the bath and mass transfer have different length scales, mass transfer is about two orders of magnitude higher in comparison with the mixing time. Niu et al. [11] reported an expression for the volumetric mass transfer coefficient (k) as a function of both the gas flow rate and the nozzle radial position. Zhang et al. [12] reported a minor effect of the bubble diameter on k. Ji et.al. [13] developed a CFD model that accurately describes mass transfer, including the dynamics in the interfacial area. However, except for our work, there are few updated reports that describe the complex nature of mass transfer due to bottom gas injection. As indicated in our previous work [5], most of the relationships of mass transfer are limited to investigate the effect of the gas flow rate, deriving expressions similar to the following one:

$$kA = C \sqrt{Q} \quad (5)$$

For example, in the work reported by Paul and Ghosh [15] the value of the constant is equal to 18.2 for bottom blowing and 9.4 for top blowing.

In our previous work, we added the effect of the slag thickness (using numerical modelling) and the porous plug radial position (using experimental and numerical modelling), obtaining the following relationships [11,14]:

$$kA = 0.0586\, Q^{0.459} \times h_s^{0.612} \quad (6)$$

$$kA = 0.0526\, Q^{0.759} \left(\frac{r}{R}\right)^{-0.066} \quad (7)$$

Ho et al. [16] also reported a review on gas–liquid mass transfer; however, different systems have different sets of variables, in this case, stirring is not carried out by a gas but with the use of impellers.

The objective of this work is to identify the optimum bottom gas injection conditions to improve the rate of mass transfer of impurities from liquid steel to liquid slag, employing two porous plugs, as a function of the gas flow rate, the porous plug position (radial position and separation angle), the slag thickness, and the ladle aspect ratio.

2. Experimental Work

2.1. Similarity

A water model was designed based on a ladle of 210 tons, with a geometric scale ratio of 1:10 (λ = 0.1). The flow rate in the water model was defined based on dynamic similarity, defined by equivalent Froude numbers between the water model and the prototype, which reduces to the following expression [17]:

$$Q_m^{STP} = \lambda^{2.5} \cdot Q_p^{TP} = 3.5\, \lambda^{2.5} \cdot Q_p^{STP} = (3.5)(0.0031) \cdot Q_p^{STP} = 0.011 \cdot Q_p^{STP} \quad (8)$$

where Q_m^{STP} is the gas flow rate in the water model at STP conditions, λ is the geometric scale ratio, and Q_p^{STP} is the gas flow rate in the prototype at STP conditions.

Table 1 summarizes the dimensions of the prototype and the water model, and it also includes the range of the variables investigated. The ladle is a cylinder with a slight conicity. The aspect ratio was defined as the height of liquid steel with respect to the

average diameter (bottom diameter and diameter at the height of the liquid steel). A total of 36 experiments were carried out. Twenty experiments to study the effect of the gas flow rate (from 0.7 to 9.26 NL/min) and the porous plug radial position (r/R from 0 to 0.5), keeping constant the aspect ratio (H_w/D = 0.8), the slag thickness (3%), and the separation angle (180°). Additionally, 16 experiments were carried out to study the effect of the aspect ratio (H_w/D = 0.8 and 1.0), the slag thickness (3 and 5%), and the separation angle (45° to 180°). The gas flow rate corresponds to the total gas flow rate injected with two porous plugs, it was divided into equal flowrates, except for the central position. The range of the variables investigated is in accordance with the similarity principles. The dimensions follow geometric similarity: the height of liquid steel, the ladle diameter, the H_w/D ratio, etc. The gas flow rate is in accordance with dynamic similarity, defined by Equation (4). The typical slag thickness in the ladle furnace is about 3%, this value is relative to the height of liquid steel, it depends on the carryover slag from the steelmaking reactor during tapping. A large value, above 5%, would imply problems with the tapping system and, therefore, a large carryover slag.

Table 1. Dimensions of the prototype and the water model, and the range of variables.

Dimensions/Variables	Prototype (p)	Water Model (m)
Diameter of bottom (D_{bottom}), m	3.513	0.351
Diameter of top (D_{top}), m	3.900	0.390
Diameter top of steel bath ($D_{top\ steel}$), m	3.663	0.366
Total height (H_{tot}), m	5.000	0.500
Height of liquid steel (H_w), m	2.833	0.283, 0.351
Number of porous plugs, –	2	2
Aspect ratio, H_w/D	0.8	0.8, 1.0
Slag thickness (h_s), %	3	3, 5
Gas flow rate (Q), NL/min	70–850	0.7, 1.85, 3.5, 7.4, 9.26
Radial position (r/R), –	0.5	0, 0.3, 0.5, 0.7
Separation angle (θ), degrees	180	45, 60, 120, 180

2.2. Experimental Set Up

Figure 1 is a schematic representation of the experimental layout. It consists of a compressor and two mass flow meters, which independently control the gas flow rate for each gas injection device. The position of the porous plugs at the bottom of the ladle is shown in Figure 2. This layout can be employed for one or multiple injection points, with central and eccentric gas injection.

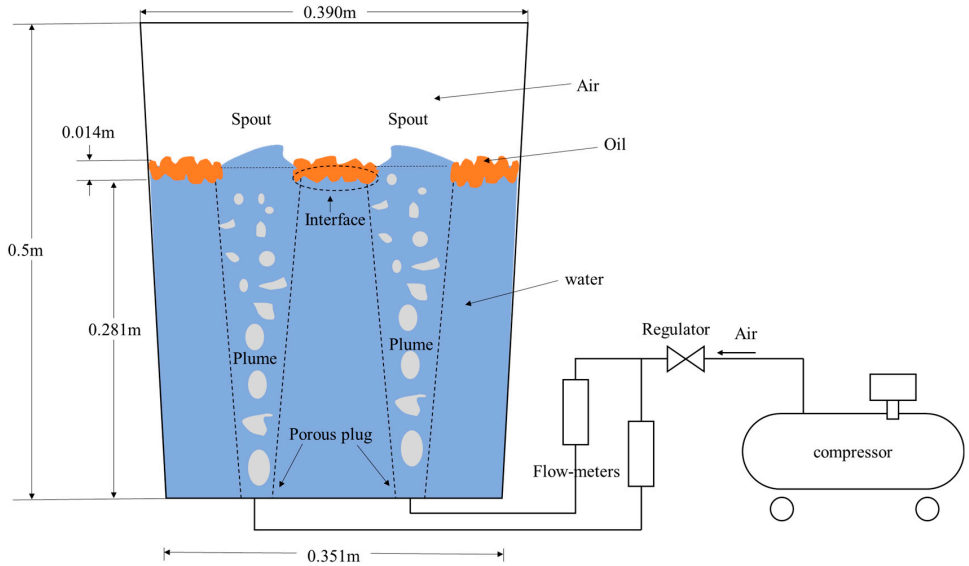


Figure 1. Schematic of the experimental setup.

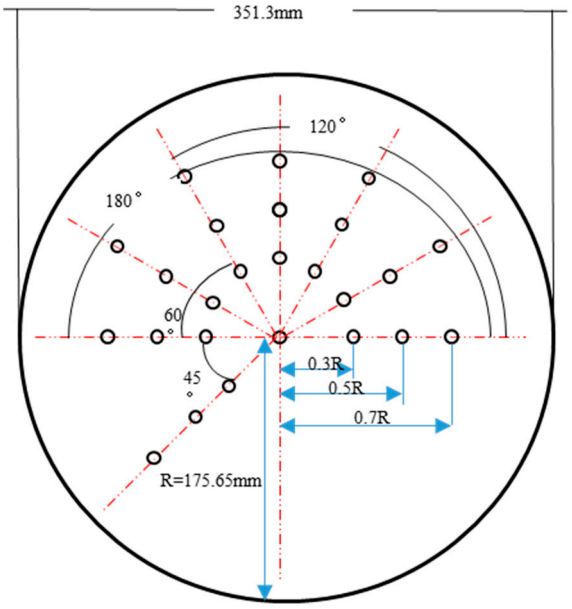


Figure 2. Porous plug positions at the bottom of the ladle.

Each porous plug has a diameter of 15 mm, and consists of 76 holes with a diameter of 1 mm, as shown in Figure 3.

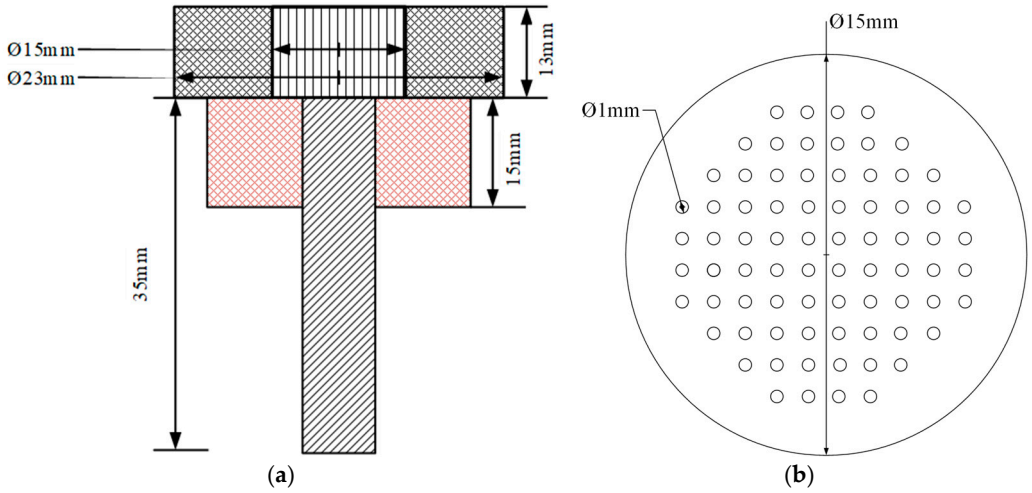


Figure 3. Porous plug: (**a**) dimensions, (**b**) top view.

The oil selected to reproduce the liquid slag was petroleum ether. This oil gave a faster response as explained in more detail in a previous work [11]. Thymol (produced by Energy Chemical Reagent Co., Ltd, Anhui, China) was also selected to represent sulfur in liquid steel. Its maximum solubility in water at 20 °C is 900 ppm [18]. In a previous work, a large number of oils were tested: paraffin oil, cotton seed oil, olive oil, silicone oil, hexane oil, pentane oil, and petroleum ether. With most oils, reaching a steady state took more than 4 h or its volatility was too high, for this reason, petroleum ether was chosen to reproduce the top slag layer. On the other hand, an ideal tracer to represent the transfer of impurities from the steel into the slag should have a high partition ratio to guarantee mass transfer control by metal phase resistance and a high solubility in the slag. Thymol ($C_{10}H_{14}O$) has a high partition ratio, which is the concentration of the impurity in the slag with respect to its concentration in the metal. The diffusion coefficient of thymol in water is small, which makes the experiments take a relatively long time.

In all the experiments, the initial concentration was 100 ppm, which is typical of ladle furnace operations; furthermore, the partition ratio of thymol in petroleum ether was 35 and the diffusion coefficient was in a similar order of magnitude to the sulfur in the steel/slag system. Table 2 summarizes the physical properties of the fluids employed in the experiments.

Table 2. Physical properties of fluids employed in the experiments.

Physical Parameter	Value
Density of water	998.2 $kg \cdot m^{-3}$
Density of air	1.225 $kg \cdot m^{-3}$
Density of petroleum ether	640 $kg \cdot m^{-3}$
Density of thymol	997.0 $kg \cdot m^{-3}$
Viscosity of water	0.001 Pa·s
Viscosity of air	1.784×10^{-5} Pa·s
Viscosity of petroleum ether	0.003 Pa·s
Diffusion coeff. of thymol in water	6.8×10^{-10} $m^2 \cdot s^{-1}$
Diffusion coeff. of thymol in oil	6.8×10^{-12} $m^2 \cdot s^{-1}$

The concentration of thymol was measured using an UV-spectrophotometer (Nanbei, China) with a wavelength range from 190 to 1100 nm (the working wavelength for the experiments was 287 nm) (Figure 4). Its wavelength resolution is 0.1 nm and it has a precision in concentration of 0.01 ppm. Standards of known concentrations were prepared to calibrate the equipment, plotting absorbance versus concentration. The absorbance ranged from about 0.05 to 0.25 for a concentration of thymol from 20 to 200 ppm, yielding a linear relationship. Preheated water was used to prepare the standards and assist the dissolution of thymol.

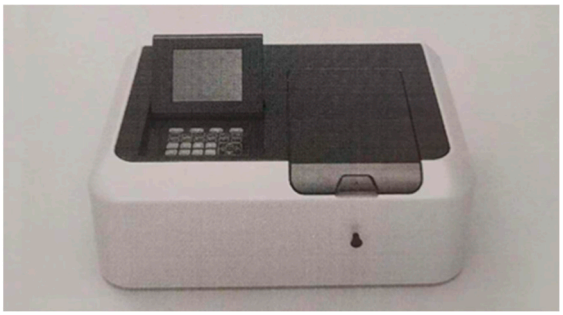


Figure 4. Ultraviolet spectrophotometer.

2.3. Computation of the Volumetric Mass Transfer Coefficient

In a typical experiment, deionized water was added to the ladle model to reach a height of 281 mm (28.92 L) or 351 mm (36.64 L), depending on the aspect ratio. The initial concentration of thymol in each experiment was 100 ppm. The amount of thymol, about 290 mg, is first dissolved in warm water to improve its dissolution rate. The oil, petroleum ether, was slowly poured on top of the water. The thickness for 3% and 5% and $H_w/D = 0.8$ was 8.4 mm and 14 mm, respectively; for an aspect ratio of $H_w/D = 1.0$, the corresponding values were 11 mm and 17.5 mm.

The gas flow rate was controlled with gas flowmeters, then, at regular intervals, samples of water were taken and analyzed using the UV-spectrophotometer to measure the concentration of thymol as a function of time. Initially, some experiments were repeated; however, due to their high reproducibility, most cases were not repeated. All the experiments were carried out at room temperature.

The computation of the volumetric mass transfer coefficient was carried out using the experimental results of concentration versus time, assuming first-order kinetics:

$$\frac{dC_w}{dt} = \frac{k_w A}{V_w}(C_w - C_w^*) \tag{9}$$

where C_w represents the concentration of thymol in deionized water, $g \cdot cm^{-3}$; k_w represents the mass transfer coefficient of thymol in water, $m \cdot s^{-1}$; A represents the contact area between petroleum ether and water, cm^2; V_w represents the volume of water, cm^3; and t represents time, s. Since the interfacial area is unknown, the term $(k_w A)$ is defined as the volumetric mass transfer coefficient (*vmtc*) in $cm^3 \cdot s^{-1}$. Replacing the equilibrium concentration C_w^* in terms of an equilibrium partition ratio, h, defined as a ratio of the concentration of thymol in oil with respect to the concentration of thymol in water once the system approaches equilibrium, and expressing the concentration of thymol in oil in terms of its concentration in water, the following expression can be derived [14]:

$$\frac{\ln\left[\left(1+\frac{hV_w}{V_0}\right)\cdot\frac{C_w}{C_w^0} - \frac{hV_w}{V_0}\right]}{1+\frac{hV_w}{V_0}} \cdot V_W = (k_w \cdot A)\cdot t \tag{10}$$

where V_o is the volume of oil; C_w is the instantaneous concentration of thymol in water; and C_w^0 is the initial concentration of thymol in water. The partition coefficient, h, represent the equilibrium concentration ratio between thymol in oil to thymol in water. Considering that the initial concentration of thymol in water was 100 ppm (100 mg/lt), the initial mass of thymol results from multiplying this value for the total amount of water. Taking an average equilibrium concentration of thymol in water (about 55 ppm), under steady-state conditions, the mass of thymol in oil is recalculated considering the volume of oil. From the experimental data, an average value for the partition ratio of 35 was employed in the calculations. The LHS in the previous equation is a constant in each experiment. A plot of the LHS versus t yields the volumetric mass transfer coefficient, as shown in Figure 5. This process is also automatically computed in Excel.

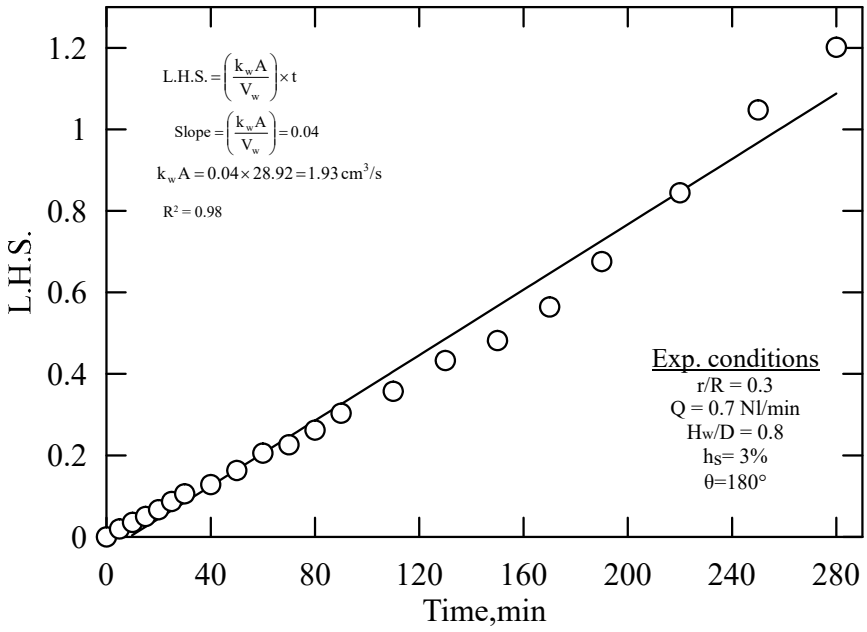


Figure 5. Computation of the volumetric mass transfer coefficient.

3. Results and Discussion

3.1. Effect of Gas Flow Rate and Radial Position on the vmtc

Figure 6 shows the experimental results for the concentration of thymol in water as a function of time at different gas flow rates and porous plug radial positions for the constant conditions of the ladle aspect ratio, the slag thickness, and the separation angle. The initial concentration rapidly decreases at the beginning and slows down at the end. This is a typical behavior for first-order kinetics. From these plots, it can be observed that the gas flow rate has a large influence on the refining rate, which increases as the gas flow rate also increases.

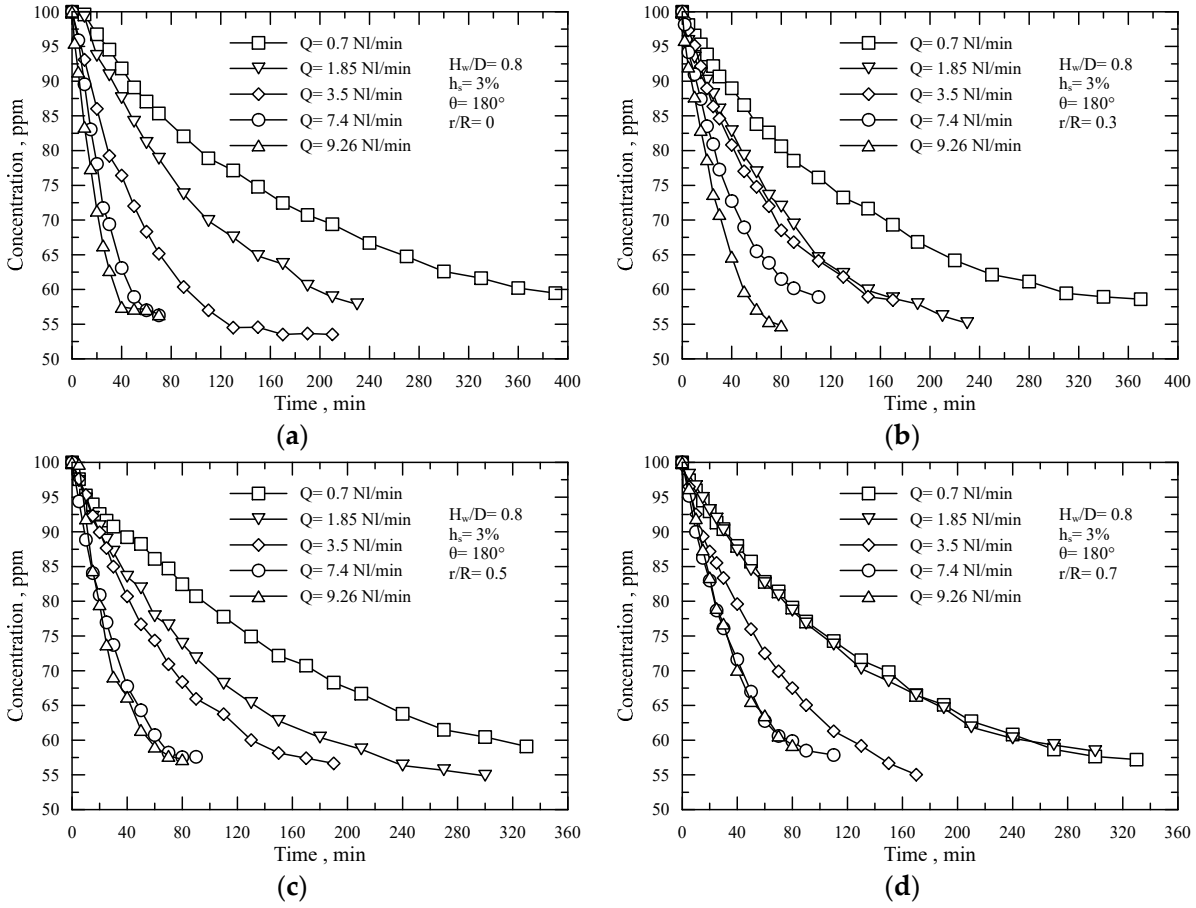


Figure 6. Thymol concentration as a function of time for different radial positions; (**a**) r/R = 0, (**b**) r/R = 0.3, (**c**) r/R = 0.5, (**d**) r/R = 0.7.

Figure 7 summarizes the effect of the porous plug radial positions at different gas flow rates. The constant values for the aspect ratio, the slag thickness, and the porous plug separation angle correspond to the values in the prototype. This plot has important results. It shows that at low flow rates, below 3.5 NL/min, the effect of the porous plug radial position has a small effect on k_wA; however, when the gas flow rate is above 7.2 NL/min, moving the porous plugs from the center to the wall decreases the volumetric mass transfer coefficient. In other words, at high gas flow rates, the best location, in terms of mass transfer, is central gas injection. One explanation as to why central gas injection, for the same gas flow rates, yields higher mass transfer rates in comparison with eccentric positions is the higher mixing intensity in the upper layer, which results in lower dead volumes [6]. Central gas injection results in a symmetric and uniform motion of the upper liquid.

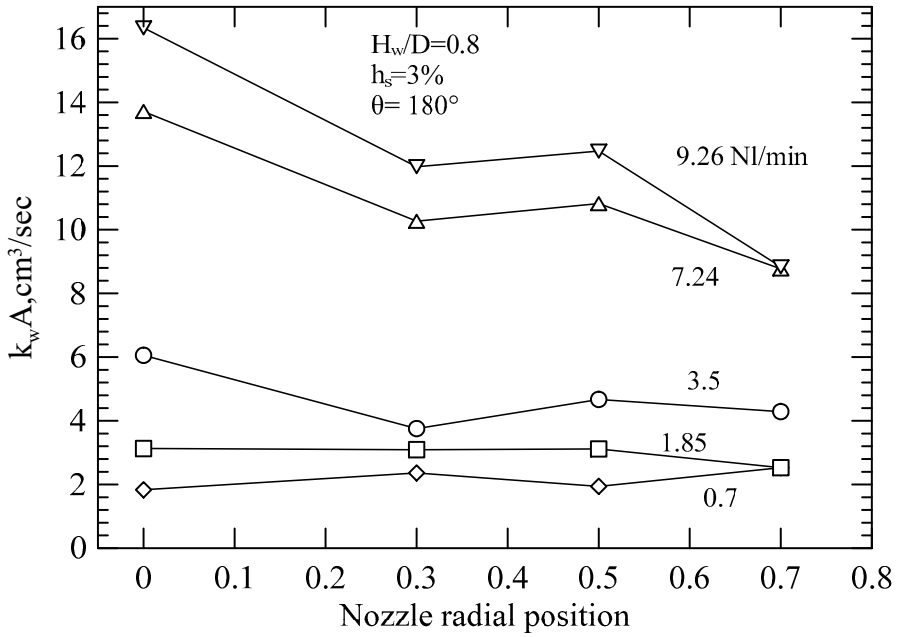


Figure 7. Effect of the radial position on the volumetric mass transfer coefficient for different gas flow rates.

The behavior with either one or two porous plugs is quite similar. The main difference with the results reported by Niu et al. [11] with one injection device is the magnitude of the mass transfer coefficient. With two injection elements the total gas flow rate can be increased, which further increases mass transfer. The maximum volumetric mass transfer coefficient with "two porous plugs" was slightly above 16 cm^3/s, which was achieved with the highest flow rate, 9.2 NL/min, and central gas injection. It should be noted that in order to compare two porous plugs at the same gas flow rate for different porous plug radial positions (r/R), from 0 to 0.7, the two porous plugs for central gas injection merge into one porous plug; therefore, the comparison with central gas injection and eccentric positions is between one and two porous plugs operating at the same gas flow rate. In order to define the best layout in terms of the gas flow rate and the radial position, we should also evaluate the practical aspects of these results. One of the disadvantages of an operation with one porous plug is that it is not possible to inject gas at a very high flow rate. The reason is the limitation on the production of a higher slag eye area when the gas flow rate increases, which promotes the absorption of gases and heat losses. The slag eye area always increases when the gas flow rate increases [19,20]. With two porous plugs, the total gas flow rate can be increased; however, the total flow rate is divided, usually in equal parts. For the industrial ladle investigated, a maximum gas flow rate per porous plug in the water model would be about 3.5 NL/min, without the formation of a slag eye area; therefore, when the gas flow rate is increased to 7.2 NL/min and one porous plug injects this amount of gas, it yields a higher mass transfer in comparison with other radial positions, but also produces a high slag eye area, becoming an unsuitable condition. Therefore, due to significant reoxidation using high gas flow rates with one porous plug that is centrally located, even if it gives a higher mass transfer coefficient, it is better to use an off-center location at the same high gas flow rate. The next radial position that gives high mass transfer rates at high gas flow rates is at the half radius and, therefore, is a better option because the total flow rate is split by half, which decreases the slag eye per porous plug and maintains a high gas flow rate. On the other hand, a radial position of two porous plugs at a half radius has the additional advantage of higher mixing conditions in liquid steel [21].

Figure 8 is an alternate representation of the previous results in order to better visualize the effect of the gas flow rate on the *vmtc*. The two lines in this plot collect the whole set of experimental data. It can be observed that, in the entire range of gas flow rates investigated, there are two slopes. These slopes were added manually to fit most of the experimental data. It can be observed that increasing the gas flow rate also increases the mass transfer coefficient, but the intensity of this effect is higher when the gas flow rate is above 1.8 NL/min. The second slope in this figure has been attributed to slag emulsification.

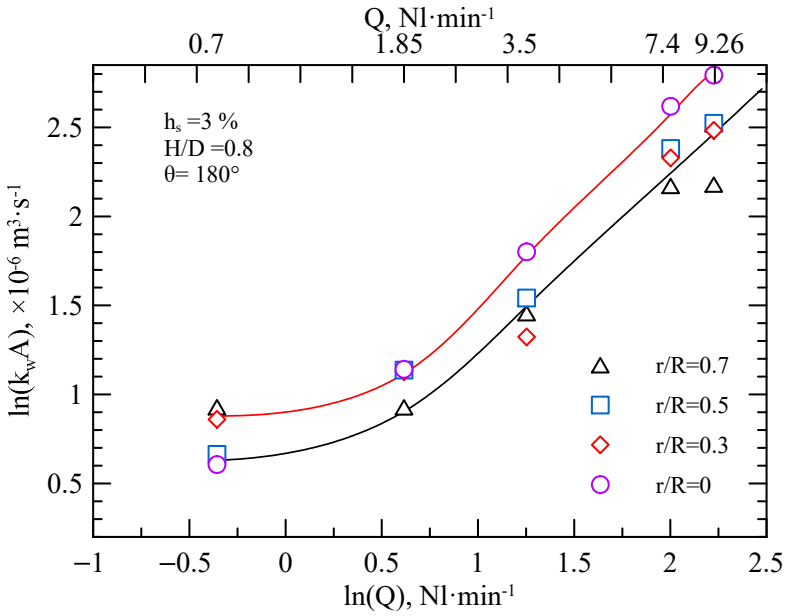


Figure 8. Effect of the gas flow rate on the volumetric mass transfer coefficient for different radial positions.

The previous results confirm the role assigned to the gas flow rate as the most important variable to improve the mixing phenomena, due to bottom gas injection in the ladle furnace. Consequently, in order to increase the removal of impurities, the gas flow rate should be increased. This behavior is valid independently of the number of porous plugs, the radial position, the separation angle, the slag thickness, and the ladle aspect ratio. The rest of the variables also play a big role in mass transfer but the behavior is more complex, as will be discussed below.

3.2. Effect of the Ladle Aspect Ratio, the Slag Thickness, and the Porous Plug Separation Angle on the vmtc

Figure 9 shows the experimental results of the concentration of thymol in water as a function of time for different ladle aspect ratios, slag thicknesses, and separation angles. The ladle aspect ratio is the ratio of the height of the liquid steel to the ladle diameter. The slag thickness is defined as the height of slag with respect to the height of the liquid steel, as a percentage. The results are valid for constant conditions of the gas flow rate (2.5 NL/min) and the porous plug radial position (r/R = 0.5). It can be observed that the end time is different for different experiments and the reason is that each experiment was stopped when it reached steady-state conditions; therefore, there was no need to repeat a final constant concentration.

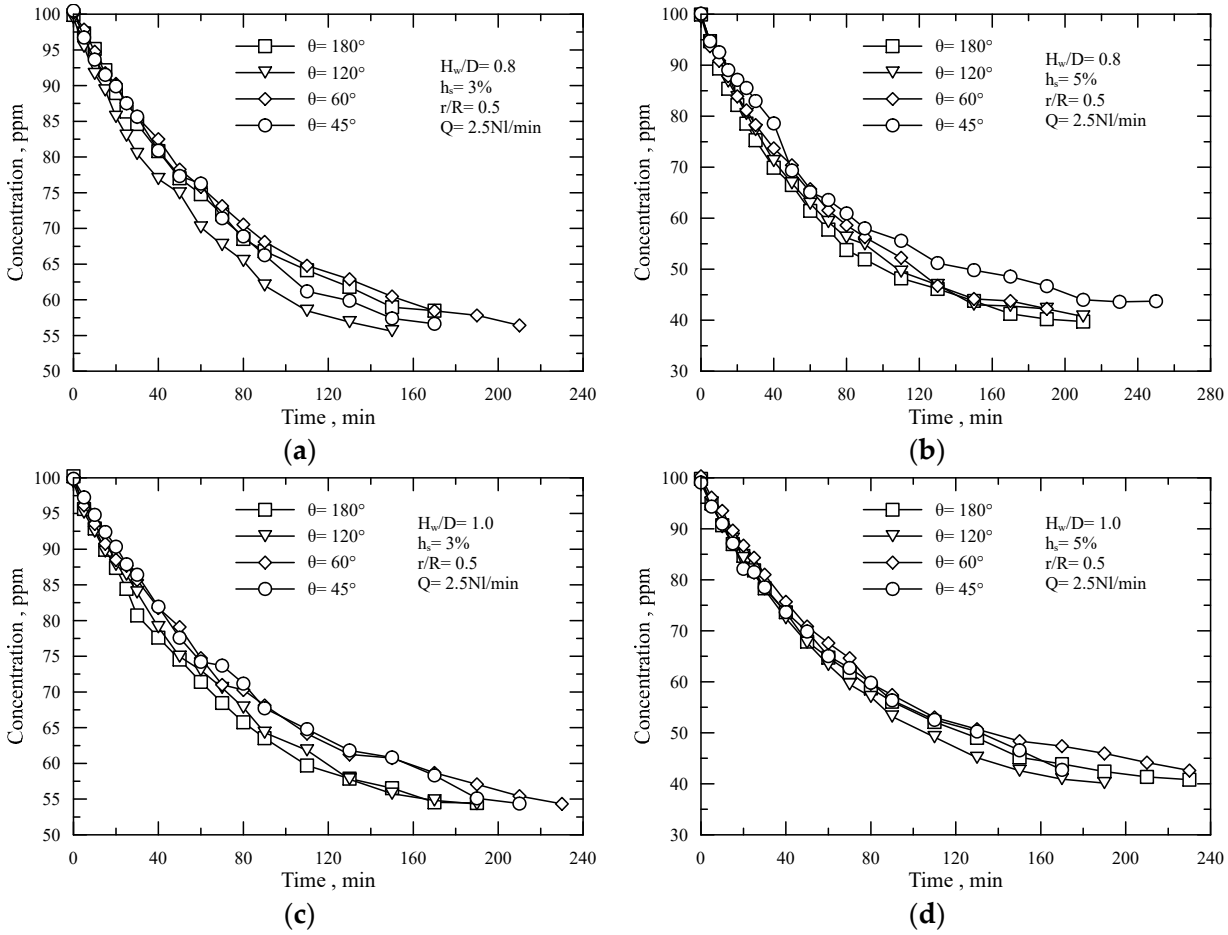


Figure 9. Thymol concentration as a function of time for different separation angles, slag thicknesses, and ladle aspect ratios; (**a**) $H_W/D = 0.8$, $h_s = 3\%$, (**b**) $H_W/D = 0.8$, $h_s = 5\%$, (**c**) $H_W/D = 1.0$, $h_s = 3\%$, (**d**) $H_W/D = 1.0$, $h_s = 5\%$.

From these plots, it can be observed that by increasing the separation angle from 45 to 180 degrees, there is also an increment in the refining rate; however, this increment is small compared with the influence of the gas flow rate or the radial position. It can also be observed that increasing the slag thickness from 3 to 5% increases the removal of impurities, with final values of 55 ppm and 40 ppm, respectively. This behavior is due to a higher slag volume and, with that, a higher refining capacity.

Figure 10 evaluates the effect of the separation angle on the volumetric mass transfer coefficient for different slag thickness and ladle aspect ratios. The results are valid for a radial position of r/R=0.5 and a gas flow rate of 2.5 NL/min. The general trend is that increasing the separation angle from 45 degrees to 180 degrees increases the mass transfer. This effect is more clearly observed when the ladle aspect ratio or slag thickness are higher. For all the conditions investigated, the highest values in mass transfer are obtained with a separation angle of 180 degrees, a ladle aspect ratio of 1.0, and a slag thickness of 5%.

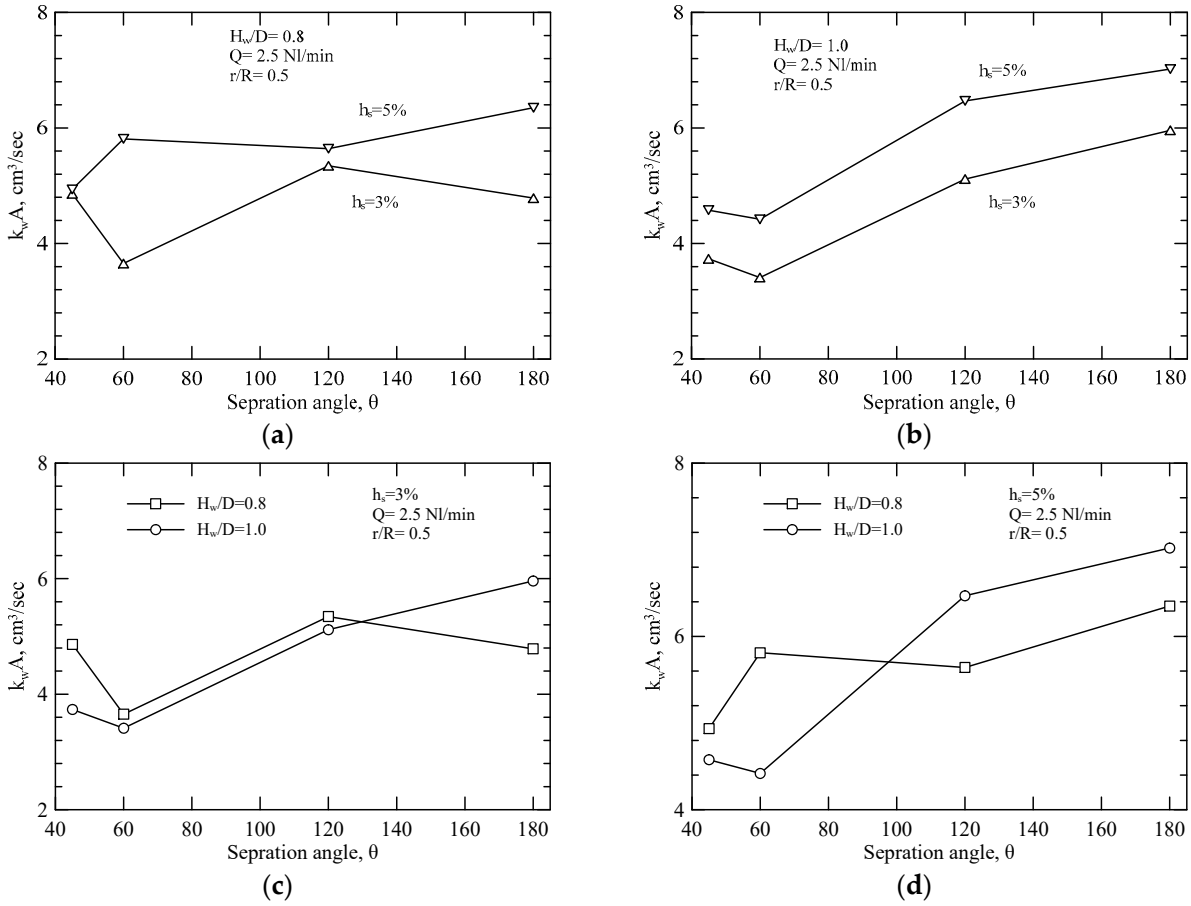


Figure 10. Effect of the separation angle for different slag thicknesses and ladle aspect ratios on the volumetric mass transfer coefficient. (**a**) H_w/D = 0.8, h_s = 3 and 5%, (**b**) H_w/D = 1.0, h_s = 3 and 5%, (**c**) h_s = 3%, H_w/D = 0.8 and 1.0, (**d**) h_s = 5%, H_w/D = 0.8 and 1.0.

Figure 11 compares the effect of the ladle aspect ratio on both the mass transfer and the mixing time. The data on the mixing time are taken from Turkoglu and Farouk [22]. They investigated the effect of the ladle aspect ratio (H_w/D) on the mixing time, reporting that increasing the H_w/D ratio from 0.5 to 1.4 linearly decreases the mixing time. The current experimental data were added to this plot, and it can be observed that as the H_w/D increases from 0.8 to 1.0, there is an increase in the mass transfer coefficient. In the figure, the plot shows a decrease in the inverse of $1/k_wA$, which is equivalent to an increase in the k_wA. In this figure, it is shown that the optimum aspect ratio in terms of mixing time is in the range from 1.2 to 1.4, while the experimental values on the mass transfer were limited to the range of 0.8–1.0. There were two reasons to limit the aspect ratio to a maximum value of 1.0; the first one is related to the actual values of the industrial size ladles, and the second is that problems that arise when the aspect ratio is above that value. The common values for the aspect ratio (H_w/D) of industrial size ladles are in the range of 0.8–1.0 [23–28]. Zhang and Chen [26] reported a large number of benefits when the aspect ratio is 1.0, such as lower weight, lower refractory consumption, lower operation costs, lower heat losses, and lower volume of dead zones. On the other hand, as the aspect ratio increases, the buoyancy forces increase, which improves the mixing intensity, but at the same time the slag/metal interfacial area decreases, which affects the slag refining rate; therefore, in practice, the upper limit is 1.0. Ladles with an aspect ratio up to 1.2 can be found [29] but this design depends on an experimental confirmation that does not increase the volume of dead zones.

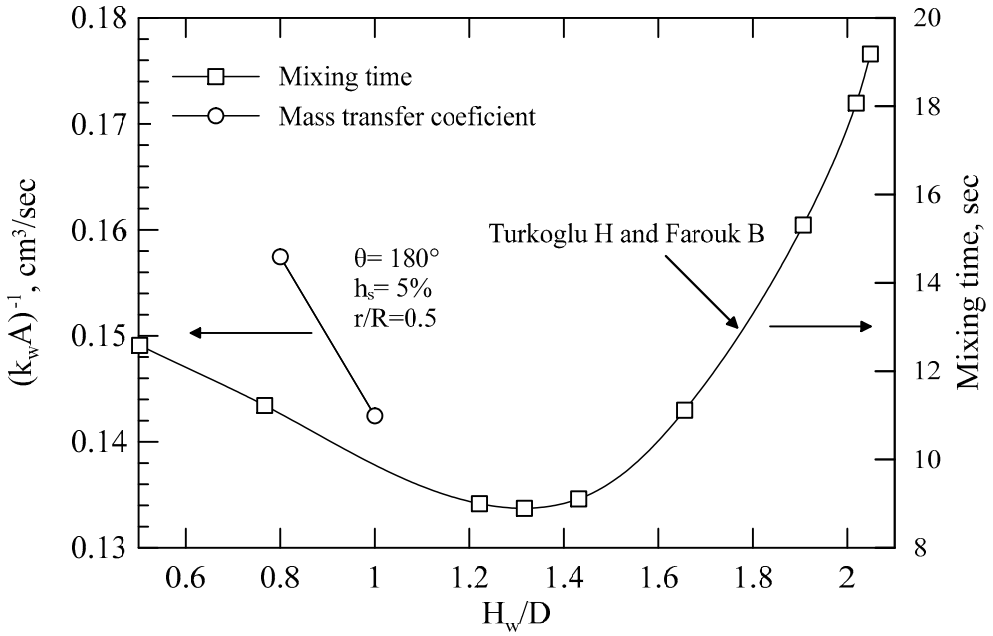


Figure 11. Comparison of the effect of the aspect ratio on the mixing time and mass transfer.

3.3. Dimensional Analysis of Experimental Data

The whole set of experimental data can be collected together using a dimensional analysis. The dependent variable is the volumetric mass transfer coefficient (k_wA) as a function of the gas flow rate (Q), the percentage of the slag thickness (h_s/H_w), the radius position of the porous plug (r), the ladle radius (R), the ladle aspect ratio (H_W), the separation angle (θ), and the gravity force (g).

$$k_wA = f\left(Q, \frac{h_s}{H_w}, r, R, \frac{H_w}{D}, \theta, g\right) \quad (11)$$

Applying the π-theorem of dimensional analysis, described in detail in reference [30], this system has eight variables and two dimensions, which results in six π-groups. Choosing as repeating variables R and Q, the following general solution is obtained:

$$\frac{k_wA}{Q} = C\,(\theta)^a\left(\frac{r}{R}\right)^b\left(\frac{H_w}{D}\right)^c\left(\frac{h_s}{H_w}\right)^d\left(\frac{gR^5}{Q^2}\right)^e \quad (12)$$

Note that in the previous equation, π_6 is the reciprocal of the Froude number $\left(\frac{gR^5}{Q^2} = \frac{1}{Fr}\right)$. Using the experimental data and a multiple regression analysis, the values of the constant and the exponents, the particular solution becomes:

$$k_wA = \left(19.9 \times 10^{-5}\right)\theta^{0.129}\left(\frac{r}{R}\right)^{-0.0101}\left(\frac{H_w}{D}\right)^{0.292}\left(\frac{h_s}{H_w}\right)^{0.604}(Fr)^{-0.160}\cdot Q \quad (13)$$

The correlation coefficient R^2 is equal to 0.65. As discussed before, in all the previous research work on mass transfer in metallurgical ladles, the mass transfer coefficient has been described as a function of Q and h_s or as function of Q and (r/R), but never before a relationship that includes five process variables, representing a significant step. The correlation coefficient can be improved with more experimental work. In this study, the number of experiments was simplified. The exponents in the dimensionless groups indicate the importance of each group; Q has an exponent of about 0.68 and, in decreasing order, is the slag thickness of 0.60, the aspect ratio of 0.29, and the separation angle of 0.13.

When all these variables increase, mass transfer also increases. The only variable that decreases mass transfer is the porous plug radial position, with an exponent equal to 0.01, an indication that in the range of the gas flow rates investigated, it has a smaller role. Finally, Figure 12 compares the predicted values using the equation with dimensionless numbers and the experimental data, observing a good agreement. It can be noticed that the prediction accuracy is higher when k_wA is below about 6.5 cm^3/s, which corresponds to low and medium gas flow rates where the slag emulsification is little or there is no slag emulsification at all. The decrease in accuracy at high values of k_wA is probably due to a higher turbulence at large flow rates and a more chaotic response.

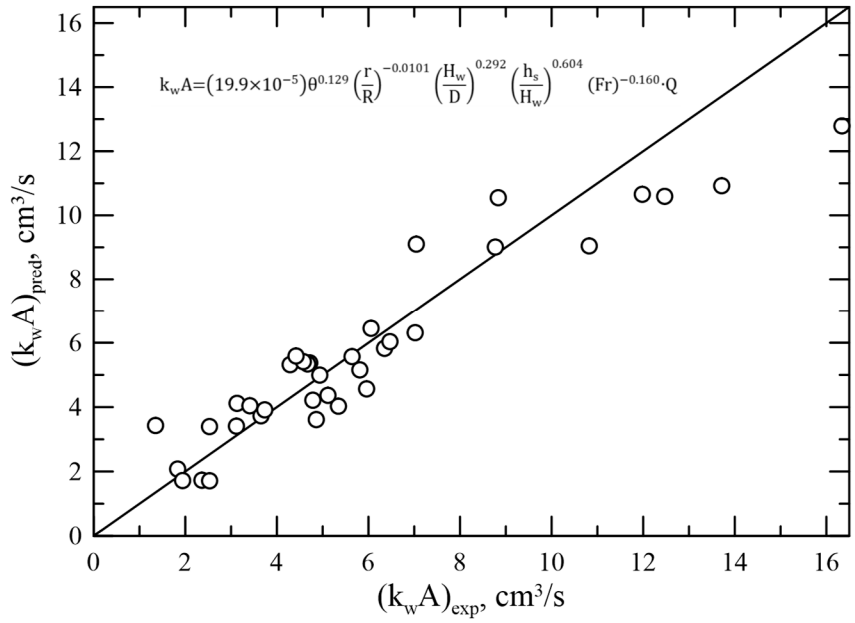


Figure 12. Comparison between the predicted and experimental values on the *vmtc* using a dimensional analysis.

The relationship derived by Abel et al. [8] was employed to evaluate the current experimental data; however, the accuracy is poor, with an average error of 55%. This is because they did not take into account the radial position and the separation angle, which play an important role.

There is still room for additional improvements in future research work in this subject. The current experimental work was performed without replicas because our preliminary work in trials at low and moderate flow rates reproduced almost identical results and there was no need for replicas; however, in light of the final analysis, it would be recommended to repeat the experiments three times at high flow rates to reach an average value that further improves the regression coefficient. Another feature that would give a better insight into the fluid dynamics of this research work is the experimental and numerical analysis of the velocity fields of the top slag layer. This work should confirm that higher rates of mass transfer are associated with a higher mixing intensity in the top slag layer. This work remains challenging due to the extremely low thickness of the top slag layer in comparison with the height of liquid steel and the ladle cylindrical shape, which makes experimental measurements complicated using PIV.

4. Conclusions

This study has investigated, through water modeling, the effect of the gas flow rate, the porous plug radial position and its separation angle, the slag thickness, and the ladle

aspect ratio on the mass transfer coefficient due to bottom gas injection with two porous plugs. The main conclusions are as follows:

The gas flow rate is the variable that has a more intense effect on the mass transfer coefficient, therefore increasing the gas flow rate will increase the mixing intensity and refining rates in steel production in the ladle furnace; however, for the same gas flow rate, the radial positions of the porous plugs can increase or decrease mass transfer. For the same gas flow rate, central gas injection increases mass transfer and decreases when the radial position moves to the walls. This effect is almost negligible when the gas flow rate is low, below the critical flow rate for gas emulsification; however, when the gas flow rate is high, there is a drastic difference between central and off-center gas injection. From this result, it would appear that central gas injection is the ideal position to improve mass transfer; however, taking into account the practical limitations related to the formation of a bigger slag eye when the gas flow rate increases imposes a smaller gas flow rate with one porous plug. Therefore, using two porous plug and a radial potion of r/R = 0.5 not only mitigates the slag eye problem operating at high gas flow rates but also provides a higher mixing intensity in liquid steel.

Increasing the slag thickness from 3 to 5%, the porous plug separation angle from 45 degrees to 180 degrees, and the ladle aspect ratio from 0.80 to 1.0 all increase the mass transfer coefficient. With the previous results, the following layout is the optimum suggested to increase mass transfer with two porous plugs: the maximum gas flow rate, a porous plug radial position at a half radius, a porous plug separation angle of 180 degrees, a 5% slag thickness, and a ladle with an aspect ratio of 1.0.

A novel equation in terms of dimensionless numbers is proposed to predict the mass transfer coefficient, which includes the effect of the variables investigated.

This work suggests a solution to the practical dilemma on a layout that simultaneously provides a high mixing intensity in the molten steel and high refining rates. The solution is to operate with two porous plugs because the total gas flow rate can be increased and then divided to decrease the slag eye area; furthermore, its radial position should be at a half radius and a separation angle of 180 degrees, which give a symmetric flow rate on the upper slag layer. The results also suggest a higher slag thickness and higher ladle aspect ratio but this should be properly controlled because a higher slag thickness increases the consumption of fluxes and a higher aspect ratio decreases the slag/metal interfacial area.

Author Contributions: Conceptualization, methodology, investigation, writing—original draft preparation, writing—review and editing, supervision, formal analysis, funding acquisition, A.N.C.; experimental work, data processing, investigation, preliminary analysis, review and editing, Z.L. All authors have read and agreed to the published version of the manuscript.

Funding: The authors are grateful for the support from the Fundamental Research Funds (Grant No. 06500108) from the University of Science and Technology Beijing, China.

Data Availability Statement: The original contributions presented in this study are included in the article. Further inquiries can be directed to the corresponding author.

Conflicts of Interest: The authors declare no conflicts of interest.

References

1. Barrington, C. The Iron Ore Challenge for Direct Reduction on Road to Carbon-Neutral Steelmaking. In *Direct from MIDREX*; MIDREX: Charlotte, NC, USA, 2022; pp. 3–7.
2. Singh, A.; Singh, V.; Patra, S.; Dixit, P.; Mukherjee, A.K. Review on High Phosphorous in Iron Ore: Problem and Way Out. *Min. Metall. Explor.* **2024**, *41*, 1497–1507. [CrossRef]
3. Holappa, L. Recent Achievements in Iron and Steel Technology. *J. Chem. Technol. Metall.* **2017**, *52*, 159–167.

4. Conejo, A.N. Physical Modeling of Bottom Gas Injection in Metallurgical Ladles: Status and Current Challenges. In Proceedings of the European Steel Technology and Application Days, Vienna, Austria, 26–29 June 2017.
5. Conejo, A.N. Physical and mathematical modelling of mass transfer in ladles due to bottom gas stirring: A review. *Processes* **2020**, *8*, 750. [CrossRef]
6. Kim, S.-H.; Fruehan, R.J. Physical Modeling of Liquid/Liquid Mass Transfer in Gas Stirred Ladles. *Metall. Trans. B* **1987**, *18*, 381–390. [CrossRef]
7. Kim, S.-H.; Fruehan, R.J.; Guthrie, R.I.L. Physical Model Studies of Two Phase Mass Transfer in Gas Stirred Ladles. In Proceedings of the 70th Steelmaking Conference Proceedings, Pittsburgh, PA, USA, 29 March–1 April 1987; pp. 107–118.
8. Abel, C.; Fruehan, R.; Vassilicos, A. Physical Modeling of Bottom-Blown Continuous Steelmaking, Part II: Development of Mass Transfer Correlations and Process Feasibility. *Iron Steelmak.* **1995**, *22*, 49–64.
9. Joubert, N.; Gardin, P.; Popinet, S.; Zaleski, S. Experimental and Numerical Modelling of Mass Transfer in a Refining Ladle. *Metall. Res. Technol.* **2022**, *119*, 109. [CrossRef]
10. Wang, X.; Liu, G.; Mu, W.; Liu, T.; Liu, K.; Wang, L. Enhancement of Mass Transfer in Converter by Improving the Flow of Slag and Molten Steel. *Phys. Fluids* **2024**, *36*, 103346. [CrossRef]
11. Niu, K.; Feng, W.; Conejo, A.N. Effect of the Nozzle Radial Position and Gas Flow Rate on Mass Transfer during Bottom Gas Injection in Ladles with One Nozzle. *Metall. Mater. Trans. B* **2022**, *53*, 1344–1350. [CrossRef]
12. Zhang, H.; Conejo, A.N.; Dutta, A.; Ramirez-Argaez, M.A.; Yan, H. Mathematical Modelling of the Liquid/Liquid Mass Transfer Behaviour in Gas Stirred Ladles. *Ironmak. Steelmak.* **2022**, *49*, 1057–1067. [CrossRef]
13. Ji, S.; Niu, K.; Conejo, A.N. Multiphase modeling of steel-slag mass transfer through distorted interface in bottom-stirred ladle. *ISIJ Int.* **2024**, *64*, 52–58. [CrossRef]
14. Hoang, Q.N.; Ramírez-Argáez, M.A.; Conejo, A.N.; Blanpain, B.; Dutta, A. Numerical modeling of liquid–liquid mass transfer and the influence of mixing in gas-stirred ladles. *JOM* **2018**, *70*, 2109–2118. [CrossRef]
15. Paul, S.; Ghosh, D.N. Model Study of Mixing and Mass Transfer Rates of Slag-Metal in Top and Bottom Blown Converters. *Metall. Trans. B* **1986**, *17*, 461–469. [CrossRef]
16. Ho, D.; Kim, K.; Earmme, T.; Kim, C. Enhancing Gas–Liquid Volumetric Mass Transfer Coefficient. *J. Ind. Eng. Chem.* **2020**, *87*, 1–17. [CrossRef]
17. Conejo, A.N.; Zhao, G.A.; Zhang, L. On the Limits of the Geometric Scale Ratio Using Water Modeling in Ladles. *Metall. Mater. Trans. B* **2021**, *52*, 2263–2274. [CrossRef]
18. PubChem Thymol Properties. Available online: https://pubchem.ncbi.nlm.nih.gov/compound/6989 (accessed on 11 November 2024).
19. Yonezawa, K.; Schwerdtfeger, K. Spout Eyes Formed by an Emerging Gas Plume at the Surface of a Slag-Covered Metal Melt. *Metall. Mater. Trans. B* **1999**, *30*, 411–418. [CrossRef]
20. Mazumdar, D.; Evans, J.W. Macroscopic Models for Gas Stirred Ladles. *ISIJ Int.* **2004**, *44*, 447–461. [CrossRef]
21. Gómez, A.S.; Conejo, A.N.; Zenit, R. Effect of Separation Angle and Nozzle Radial Position on Mixing Time in Ladles with Two Nozzles. *J. Appl. Fluid Mech.* **2018**, *11*, 11–20. [CrossRef]
22. Turkoglu, H.; Farouk, B. Mixing Time and Liquid Circulation Rate in Steelmaking Ladles with Vertical Gas Injection. *ISIJ Int.* **1991**, *31*, 1371–1380. [CrossRef]
23. Villela-Aguilar, J.D.J.; Ramos-Banderas, J.Á.; Hernández-Bocanegra, C.A.; Urióstegui-Hernández, A.; Solorio-Díaz, G. Optimization of the Mixing Time Using Asymmetrical Arrays in Both Gas Flow and Injection Positions in a Dual-Plug Ladle. *ISIJ Int.* **2020**, *60*, 1172–1178. [CrossRef]
24. González-Bernal, R.; Solorio-Diaz, G.; Ramos-Banderas, A.; Torres-Alonso, E.; Hernández-Bocanegra, C.A.; Zenit, R. Effect of the Fluid-Dynamic Structure on the Mixing Time of a Ladle Furnace. *Steel Res. Int.* **2018**, *89*, 1700281. [CrossRef]
25. Salcudean, M.; Guthrie, R.I.L. Turbulent Flow in Filling Ladles. *Metall. Trans. B* **1978**, *9*, 673–680. [CrossRef]
26. Zhang, X.; Chen, L. Study and application of ladle shape for liquid steel. *Steelmaking* **2020**, *36*, 78–81.
27. Li, Q.; Qiu, G.; Wang, G.; Gao, P.; Li, R. Numerical Simulation of Bottom Argon Blowing Process for 130 Ton Ladle. *Spec. Steel* **2024**, *45*, 59–65. [CrossRef]
28. Zhang, W.; Wu, X.; Wang, A.; Li, X.; Li, S. Design and Practice of 100 t Ladle Capacity Expansion at Tangsteel Co., Ltd. *Wide Heavy Plate* **2024**, *30*, 45–48.
29. Pistorius, P.C. Slag Carry-over and the Production of Clean Steel. *J. South. Afr. Inst. Min. Metall.* **2019**, *119*, 557–561. [CrossRef]
30. Conejo, A.N. *Fundamentals of Dimensional Analysis: Theory and Applications in Metallurgy*; Springer: Singapore, 2021; ISBN 978-981-16-1601-3.

Disclaimer/Publisher's Note: The statements, opinions and data contained in all publications are solely those of the individual author(s) and contributor(s) and not of MDPI and/or the editor(s). MDPI and/or the editor(s) disclaim responsibility for any injury to people or property resulting from any ideas, methods, instructions or products referred to in the content.